

# Vránaite, ideally $\text{Al}_{16}\text{B}_4\text{Si}_4\text{O}_{38}$ , a new mineral related to boralsilite, $\text{Al}_{16}\text{B}_6\text{Si}_2\text{O}_{37}$ , from the Manjaka pegmatite, Sahatany Valley, Madagascar

JAN CEMPÍREK<sup>1</sup>, EDWARD S. GREW<sup>2,\*</sup>, ANTHONY R. KAMPF<sup>3</sup>, CHI MA<sup>4</sup>, MILAN NOVÁK<sup>1</sup>,  
PETR GADAS<sup>1</sup>, RADEK ŠKODA<sup>1</sup>, MICHAELA VAŠINOVÁ-GALIOVÁ<sup>5</sup>, FEDERICO PEZZOTTA<sup>6</sup>,  
LEE A. GROAT<sup>7</sup>, AND SERGEY V. KRIVOVICHEV<sup>8</sup>

<sup>1</sup>Department of Geological Sciences, Masaryk University, Brno, 611 37, Czech Republic

<sup>2</sup>School of Earth and Climate Sciences, University of Maine, 5790 Bryand Center, Orono, Maine 04469 U.S.A.

<sup>3</sup>Mineral Sciences Department, Natural History Museum of Los Angeles County, 900 Exposition Boulevard, Los Angeles, California 90007 U.S.A.

<sup>4</sup>Division of Geological and Planetary Sciences, California Institute of Technology, Pasadena, California 91125, U.S.A.

<sup>5</sup>Department of Chemistry, Masaryk University, Brno, 611 37, Czech Republic

<sup>6</sup>Mineralogy Department, Museo di Storia Naturale, Corso Venezia 55, Milan, I-20121, Italy

<sup>7</sup>Earth, Ocean and Atmospheric Sciences, University of British Columbia, Vancouver, British Columbia V6T 1Z4, Canada

<sup>8</sup>Department of Crystallography, St. Petersburg State University, University Embankment 7/9, 199034 St. Petersburg, Russia

## ABSTRACT

The system  $\text{B}_2\text{O}_3$ - $\text{Al}_2\text{O}_3$ - $\text{SiO}_2$  (BAS) includes two ternary phases occurring naturally, boromullite,  $\text{Al}_9\text{BSi}_2\text{O}_{19}$ , and boralsilite,  $\text{Al}_{16}\text{B}_6\text{Si}_2\text{O}_{37}$ , as well as synthetic compounds structurally related to mullite. The new mineral vránaite, a third naturally occurring anhydrous ternary BAS phase, is found with albite and K-feldspar as a breakdown product of spodumene in the elbaite-subtype Manjaka granitic pegmatite, Sahatany Valley, Madagascar. Boralsilite also occurs in this association, although separately from vránaite; both minerals form rare aggregates of subparallel prisms up to 100  $\mu\text{m}$  long. Optically, vránaite is biaxial (-),  $n_\alpha = 1.607(1)$ ,  $n_\beta = 1.634(1)$ ,  $n_\gamma = 1.637(1)$  (white light),  $2V_\gamma(\text{calc}) = 36.4^\circ$ ,  $X \approx \mathbf{c}$ ;  $Y \approx \mathbf{a}$ ;  $Z = \mathbf{b}$ . An averaged analysis by EMP and LA-ICP-MS (Li, Be) gives (wt%)  $\text{SiO}_2$  20.24,  $\text{B}_2\text{O}_3$  11.73,  $\text{Al}_2\text{O}_3$  64.77, BeO 1.03, MnO 0.01, FeO 0.13,  $\text{Li}_2\text{O}$  1.40, Sum 99.31. Raman spectroscopy in the 3000–4000  $\text{cm}^{-1}$  region rules out the presence of significant OH or  $\text{H}_2\text{O}$ . Vránaite is monoclinic, space group  $I2/m$ ,  $a = 10.3832(12)$ ,  $b = 5.6682(7)$ ,  $c = 10.8228(12)$  Å,  $\beta = 90.106(11)^\circ$ ;  $V = 636.97(13)$  Å<sup>3</sup>,  $Z = 1$ . In the structure [ $R_1 = 0.0416$  for  $550 F_o > 4\sigma F_o$ ], chains of  $\text{AlO}_6$  octahedra run parallel to [010] and are cross-linked by  $\text{Si}_2\text{O}_7$  disilicate groups,  $\text{BO}_3$  triangles, and clusters of  $\text{AlO}_4$  and two  $\text{AlO}_3$  polyhedra. Two Al positions with fivefold coordination, Al4 and Al5, are too close to one another to be occupied simultaneously; their refined site-occupancy factors are 54% and 20% occupancy, respectively. Al5 is fivefold-coordinated Al when the Al9 site and both O9 sites are occupied, a situation giving a reasonable structure model as it explains why occupancies of the Al5 and O9 sites are almost equal. Bond valence calculations for the Al4 site suggest Li is likely to be sited here, whereas Be is most probably at the Al5 site. One of the nine O sites is only 20% occupied; this O9 site completes the coordination of the Al5 site and is located at the fourth corner of what could be a partially occupied  $\text{BO}_4$  tetrahedron, in which case the B site is shifted out of the plane of the  $\text{BO}_3$  triangle. However, this shift remains an inference as we have no evidence for a split position of the B atom. If all sites were filled (Al4 and Al5 to 50%), the formula becomes  $\text{Al}_{16}\text{B}_4\text{Si}_4\text{O}_{38}$ , close to  $\text{Li}_{1.08}\text{Be}_{0.47}\text{Fe}_{0.02}\text{Al}_{14.65}\text{B}_{3.89}\text{Si}_{3.88}\text{O}_{36.62}$  calculated from the analyses assuming cations sum to 24. The compatibility index based on the Gladstone–Dale relationship is 0.001 (“superior”). Assemblages with vránaite and boralsilite are inferred to represent initial reaction products of a residual liquid rich in Li, Be, Na, K, and B during a pressure and chemical quench, but at low  $\text{H}_2\text{O}$  activities due to early melt contamination by carbonate in the host rocks. The two BAS phases are interpreted to have crystallized metastably in lieu of dumortierite in accordance with Ostwald Step Rule, possibly first as “boron mullite,” then as monoclinic phases. The presence of such metastable phases is suggestive that pegmatites crystallize, at least partially, by disequilibrium processes, with significant undercooling, and at high viscosities, which limit diffusion rates.

**Keywords:** Vránaite, boralsilite, Madagascar, pegmatite, new mineral, structural complexity, Ostwald step rule, borosilicate minerals

## INTRODUCTION

The system  $\text{B}_2\text{O}_3$ - $\text{Al}_2\text{O}_3$ - $\text{SiO}_2$  (BAS, Fig. 1) includes two ternary phases occurring naturally, boromullite,  $\text{Al}_9\text{BSi}_2\text{O}_{19}$ , and boralsilite,  $\text{Al}_{16}\text{B}_6\text{Si}_2\text{O}_{37}$ , as well as numerous binary and ternary synthetic compounds structurally related to mullite, some of which

are suitable for a wide range of applications as refractory materials because of their high-temperature stability, low-thermal expansion, high-chemical stability, high-creep resistance, and other desirable properties (e.g., Fischer and Schneider 2008; Schneider et al. 2008; Gatta et al. 2010, 2013). One such phase,  $\text{Al}_{16}\text{B}_4\text{Si}_4\text{O}_{38}$ , was synthesized by Werding and Schreyer (1992), who characterized it as an orthorhombic “B-bearing derivative of sillimanite,” and predicted

\* E-mail: esgrew@maine.edu

that it could be found in nature. However, in re-indexing its powder XRD pattern with a mullite cell, Grew et al. (2008) obtained cell parameters very similar to those for “boron-mullite.” Lührs et al. (2014) synthesized an orthorhombic phase  $\text{Al}_{16.8}\text{B}_{3.6}\text{Si}_{3.7}\text{O}_{38}$  and successfully refined its structure using the Rietveld method to show it to be closely related to mullite. Novák et al. (2015) reported a naturally occurring phase with the approximate composition  $\text{Al}_{16}\text{B}_4\text{Si}_4\text{O}_{38}$ , which occurs with boralsilite in the Manjaka pegmatite, Sahatany Valley, Madagascar. Crystallographic study showed that the Manjaka mineral has a structure more closely related to that of boralsilite than to mullite. The mineral is sufficiently distinct chemically from boralsilite to qualify as new. We have named the new borosilicate vránaite for Stanislav Vrána (born 1936), a scientist with the Czech Geological Survey, and an excellent petrologist who, besides numerous other works, has studied petrology and mineralogy of borosilicate minerals. The mineral and its name have been approved by the International Mineralogical Association Commission on New Minerals, Nomenclature and Classification (IMA 2015-84, Cempírek et al. 2016).

The holotype crystal (grain 1) used for single-crystal diffraction and optical measurements is deposited in the Natural History Museum of Los Angeles County under number 65609. Other parts of the holotype are deposited in the collection of the Department of Mineralogy and Petrography, Moravian Museum, Brno, Czech Republic under numbers B11277 (thin sections from which the holotype crystal was extracted) and B11278 (rock sample from which the thin section was prepared).

## METHOD

X-ray powder diffraction data were recorded using a Rigaku R-Axis Rapid II curved imaging plate microdiffractometer with monochromatized  $\text{MoK}\alpha$  radiation at the Natural History Museum of Los Angeles County. A Gandolfi-like motion on the  $\varphi$  and  $\omega$  axes was used to randomize the sample. Observed  $d$ -spacings and intensities were derived by profile fitting using JADE 2010 software (Materials

Data, Inc.). Data (in Å for  $\text{MoK}\alpha$ ) are given in Table 1. Unit-cell parameters were refined from the powder data using JADE 2010 with whole pattern fitting (Table 1).

Single-crystal X-ray studies were carried out using the same diffractometer and radiation noted above (Table 2). The Rigaku CrystalClear software package was used for processing of structure data, including the application of an empirical multi-scan absorption correction using ABSCOR (Higashi 2001). The structure was solved using SIR2011 (Burla et al. 2012). SHELXL-97 software (Sheldrick 2008) was used for the refinement of the structure.

Single-crystal electron backscatter diffraction (EBSD) analyses at a sub-micrometer scale were performed using an HKL EBSD system on the ZEISS 1550VP scanning electron microscope operated at 20 kV and 4 nA in a focused beam with a 70° tilted stage in variable pressure mode (20 Pa) at Caltech, following the method described in Ma and Rossman (2008, 2009). The EBSD system was calibrated using a single-crystal silicon standard.

Raman spectra of vránaite and reference minerals (boralsilite, muscovite) were acquired on LabRAM HR Evolution (Horiba, Jobin Yvon) Raman spectrometer system, at the Department of Geological Sciences, Masaryk University, Brno. The Raman spectra were excited by 532 nm Nd:YAG and 633 nm He-Ne lasers and collected in a range between 3000 and 4000  $\text{cm}^{-1}$  with a resolution of 1  $\text{cm}^{-1}$ . The laser spot for the 100× objective used provides approximately <1  $\mu\text{m}$  lateral and 2  $\mu\text{m}$  horizontal resolution. Repeated acquisitions were accumulated to improve spectral signal-to-noise ratio. No surface damage was observed after the laser illumination during the measurement.

Chemical data for boralsilite and vránaite obtained by electron microprobe analysis (EMPA) and by laser ablation-inductively coupled plasma-mass spectroscopy (LA-ICP-MS) are taken from Novák et al. (2015), and thus only selected features of the analytical method are repeated here. The two minerals were analyzed with a Cameca SX100 electron microprobe at the Joint Laboratory of Electron Microscopy and Microanalysis, Department of Geological Sciences, Masaryk University, Brno, and Czech Geological Survey, Brno, in wavelength-dispersive mode, with accelerating voltage 15 kV, beam current 10–20 nA, and spot size ~2–5  $\mu\text{m}$ . The following standards and X-ray  $K\alpha$  lines were used: danburite (B), sanidine (Si, Al), albite (Na), almandine (Fe), spessartine (Mn), and topaz (F). The peak counting time was 10 s for major elements and 20–40 s for minor elements. The background counting time was

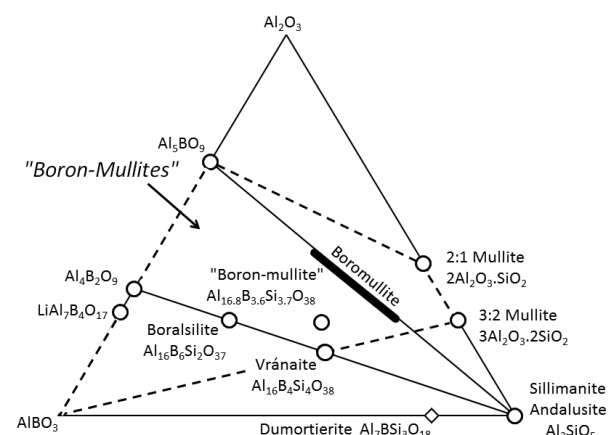


**FIGURE 1.** Phases related to mullite (circles), including boromullite (bar), together with dumortierite (diamond), plotted in the  $\text{Al}_2\text{O}_3$ - $\text{AlBO}_3$ - $\text{Al}_2\text{SiO}_5$  of the  $\text{Al}_2\text{O}_3$ - $\text{B}_2\text{O}_3$ - $\text{SiO}_2$  (BAS) system. Sources of data: field of “boron-mullites” (dashed lines, Werdning and Schreyer 1996); boromullite polysomatic series (Buick et al. 2008); “boron-mullite,”  $\text{Al}_{16.8}\text{B}_{3.6}\text{Si}_{3.7}\text{O}_{38}$  (Lührs et al. 2014),  $\text{LiAl}_7\text{B}_4\text{O}_{17}$  (Åhman et al. 1997), dumortierite end-member (Piecicka et al. 2013); vránaite (this study); other mullite-related phases (Fischer and Schneider 2008; Grew et al. 2008).

<sup>1</sup>Deposit item AM-16-95686, Supplemental Material, Table 1, and CIF. Deposit items are free to all readers and found on the MSA web site, via the specific issue’s Table of Contents (go to <http://www.minsocam.org/MSA/AmMin/TOC/>).

**TABLE 2.** Data collection and structure refinement details for vránaite<sup>a</sup>

Diffractometer	Rigaku R-Axis Rapid II
X-ray radiation/power	$\text{MoK}\alpha$ ( $\lambda = 0.71075$ Å)/50 kV, 40 mA
Temperature	293(2) K
Formula from refined occupancies	$\text{Al}_{14.96}\text{B}_3\text{Si}_{3.683}$
Space group	$I2/m$
Unit-cell dimensions	$a = 10.3832(12)$ Å $b = 5.6682(7)$ Å $c = 10.8228(12)$ Å $\beta = 90.106(11)^\circ$
V	$636.97(13)$ Å <sup>3</sup>
Z	1
Density for $\text{Li}_{1.08}\text{Be}_{0.47}\text{Fe}_{0.02}\text{Al}_{14.65}\text{B}_{3.89}\text{Si}_{3.88}\text{O}_{36.62}$	2.986 $\text{g/cm}^3$
Absorption coefficient	0.925 $\text{mm}^{-1}$
$F(000)$	565.1
Crystal size	$35 \times 30 \times 20$ $\mu\text{m}$
$\theta$ range	$3.93$ to $24.95^\circ$
Index ranges	$-12 \leq h \leq 12$ , $-6 \leq k \leq 6$ , $-12 \leq l \leq 10$
Reflections collected/unique	2308/620; $R_{\text{int}} = 0.048$
Reflections with $F_o > 4\sigma(F_o)$	550
Completeness to $\theta = 24.95^\circ$	98.9%
Refinement method	Full-matrix least-squares on $F^2$
Parameter/restraints	102/0
GoF	1.094
Final R indices [ $F_o > 4\sigma(F_o)$ ]	$R_1 = 0.0416$ , $wR_2 = 0.0986$
R indices (all data)	$R_1 = 0.0478$ , $wR_2 = 0.1024$
Largest diff. peak/hole	+0.69/−0.51 $\text{e} \text{ \AA}^{-3}$

Notes: The structural formula is calculated as a sum of refined site occupancies (i.e., numbers of electrons), with no attempt to balance charge. The large negative charge sum (−0.773) is related to the presence of Li and Be in part of Al sites. <sup>a</sup>  $R_{\text{int}} = \frac{\sum |F_o^2 - F_c^2|}{\sum F_o^2}$ ,  $\text{GoF} = S = \frac{[\sum (w(F_o^2 - F_c^2)^2)]^{1/2}}{(n - p)^{1/2}}$ ,  $R_1 = \frac{\sum |F_o - |F_c||}{\sum |F_o|}$ ,  $wR_2 = \frac{[\sum (w(F_o^2 - F_c^2)^2)]^{1/2}}{[\sum (w(F_o^2)^2)]^{1/2}}$ ;  $w = 1/(\sigma^2(F_o^2) + (aP)^2 + bP)$ , where  $a$  is 0.0229,  $b$  is 6.3767, and  $P$  is  $[2F_o^2 + \text{Max}(F_c^2, 0)]/3$ .

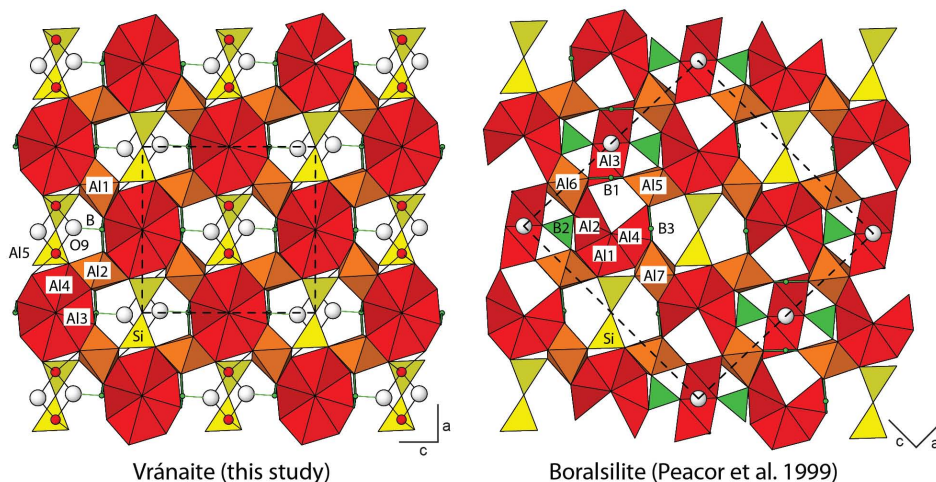


**FIGURE 2.** Crystal structure of vránaite and comparison with boralsilite. The two structures are oriented such that the  $\text{Si}_2\text{O}_7$  units (shown in yellow) are parallel. The A15 (red spheres) and O9 (white spheres) sites are only 20% occupied in vránaite. The B2 site (green triangles) is in tetrahedral coordination in boralsilite; cf. B-O9 in vránaite.

one-half of the peak counting time on the high- and low-energy background positions. Boron was analyzed in peak-area mode on a  $\text{BK}\alpha$  line using accelerating voltage 5 kV, beam current 100 nA, and beam diameter 10  $\mu\text{m}$ , and a Ni/C multilayered monochromator with  $2d = 95 \text{ \AA}$  (PC2 in terms of CAMECA). Peak-area integration was carried out in the range 62–73  $\text{\AA}$  for 240 s over 1000 steps. The first and the last 75 steps were used for background determination. Data were processed using the X-Phi matrix correction of Merlet (1994). The detection limit for B is  $\sim 2500$  ppm and the relative error expressed as  $3\sigma$  is  $\sim 10$  rel% for 15 wt%  $\text{B}_2\text{O}_3$  content. We chose to operate in peak area mode because of the effect on the shape and position of the  $\text{BK}\alpha$  peak due to differences in composition and structure between standard and unknown, the most important being coordination of B (tetrahedral in danburite, but largely trigonal in the unknowns). McGee and Anovitz (1996) showed that the effect of such differences on the  $\text{BK}\alpha$  peak is reduced when peak area is measured. We did not attempt to control for crystallographic orientation of standard and unknown given that vránaite and boralsilite are finely fibrous.

LA-ICP-MS equipment at the Department of Chemistry, Masaryk University, Brno, used to determine Li, Be, and B contents in boralsilite and vránaite consists of a UP 213 (New Wave Research, Inc., Fremont, California, U.S.A.) laser-ablation system and an Agilent 7500 CE (Agilent Technologies, Santa Clara, California, U.S.A.) ICPMS spectrometer. A commercial Q-switched Nd:YAG laser ablation device works at the fifth harmonic frequency, which corresponds to the wavelength of 213 nm. Laser ablation was performed with a laser spot of diameter 55  $\mu\text{m}$ , laser fluence 9 J/cm<sup>2</sup>, and repetition rate 10 Hz. Li, Be, and B contents of elements were calculated using NIST SRM 610 and 612 standards and Al was used as an internal reference element after baseline correction and integration of the peak area.

$\text{H}_2\text{O}$  and  $\text{CO}_2$  were not determined directly as the recorded Raman spectra showed no indications of  $\text{OH}^-$ ,  $\text{H}_2\text{O}$ ,  $\text{CO}_2$ , or  $\text{CO}_3^{2-}$ .

### CRYSTAL STRUCTURE

The crystal structure of vránaite is based upon chains of edge-sharing  $\text{AlO}_6$  octahedra that run parallel to  $[010]$  and are cross-linked by  $\text{Si}_2\text{O}_7$  disilicate groups,  $\text{BO}_3$  triangles, and clusters of  $\text{AlO}_4$  and  $\text{AlO}_5$  polyhedra (Fig. 2). Two fivefold-coordinated Al sites, A14 and A15, cannot be occupied simultaneously; the refinement gives site-occupancy factors of 54 and 20% occupancy, respectively. Moreover, occupancies of A15 and O9 sites are approximately equal to 0.20; this could give the following combinations:

- (1) Threefold-coordinated Al when the A19 site is occupied and the O9 sites are empty;
- (2) Fourfold-coordinated Al when the A19 site is occupied and only one of two O9 sites is occupied;
- (3) Fivefold-coordinated Al when the A19 site and both O9 sites are occupied.

There is no problem if two O9 sites are occupied simultaneously; the O9-O9 distance is ca. 2.25  $\text{\AA}$ , which is permissible for the shared edge between two adjacent  $\text{AlO}_5$  polyhedra. Therefore, the option (3) is plausible and the structure model is very reasonable, indeed, this explains exactly why occupancies of the A15 and O9 sites are almost equal.

Bond valence calculations for the A14 site suggest that Li is likely to be sited here, whereas Be is most probably present at the A15 site. Both A14 and A15 sites are dominated by Al, i.e., occupancies of Li and Be are subordinate at their respective sites. Eight of the O sites are fully occupied, whereas the O9 site is only 20% occupied and completes the coordination of the A15 site. This site is located at the fourth corner of what could be a partially occupied  $\text{BO}_4$  tetrahedron, that is, the B site would be shifted out of the plane of the  $\text{BO}_3$  triangle. However, our refinement did not give any evidence for a split position of the B atom, so this shift remains an inference.

The refined sum of cation electron densities ( $270.48 e^-$ ) obtained from the structural formulas in Table 2 and the measured occupancies listed in Table 3 shows an excellent agreement with the  $269.85 e^-$  for the empirical formula  $\text{Li}_{1.08}\text{Be}_{0.47}\text{Fe}_{0.02}\text{Al}_{14.65}\text{B}_{3.89}\text{Si}_{3.88}\text{O}_{36.62}$  calculated from the analyses assuming cations sum to 24, an assumption justified by the total obtained if B, Si, A11, A12, and A13 were fully occupied and A14 and A15 were 50% occupied, as well as by analogy with boralsilite. Similarly, the refined number of anions matches well with that of the empirical formula (36.83 and 36.62 atoms, respectively).

In discussing the crystallographic relationships between werdingite and other phases with mullite-type structures, Niven et al. (1991) noted that one of two slabs constituting the structure of werdingite,  $(\text{Mg,Fe})_2\text{Al}_{12}(\text{Al,Fe})_2\text{Si}_4(\text{B,Al})_4\text{O}_{37}$ , has the ideal composition  $^{[6]}\text{Al}_8^{[5]}\text{Al}_4^{[4]}\text{Al}_4\text{B}_4\text{Si}_4\text{O}_{38}$ , with monoclinic symmetry ( $C2/m$ ). It appears that, both topologically and geometrically, the linkages of  $^{[6]}\text{Al}$ , Si, and B polyhedra in werdingite and vránaite are essentially identical.

Electron backscattered diffraction patterns of grains 1 (Appendix<sup>1</sup> 1) and 3 can be indexed nicely using the vránaite structure in  $C2/m$  (converted from  $I2/m$ ), with a mean angular deviation of 0.38 to 0.41°.

**TABLE 3.** Atomic coordinates, site-occupancy factors (sof), and isotropic displacement parameters ( $\text{\AA}^2$ ), with standard deviation in parentheses

Atom	x	y	z	Occupancy	$U_{\text{eq}}$
B	0.5014(6)	1/2	0.2334(8)	1	0.0248(17)
Si	0.34575(15)	0	0.49547(15)	1	0.0166(5)
Al1	1/4	1/4	3/4	1	0.0137(4)
Al2	1/4	3/4	1/4	1	0.0155(5)
Al3	-0.02458(17)	1/2	0.33947(16)	1	0.0176(5)
Al4	0.2049(3)	1/2	0.4732(3)	0.541(9)	0.0179(13)
Al5	0.3564(10)	1/2	0.4997(9)	0.199(10)	0.026(4)
O1	0.3687(4)	1/2	0.2260(3)	1	0.0141(9)
O2	0.0690(2)	0.2107(5)	0.7241(3)	1	0.0168(7)
O3	1/2	0	1/2	1	0.052(2)
O4	0.2957(3)	-0.2326(5)	0.4236(3)	1	0.0222(7)
O5	0.2855(4)	0	0.6342(4)	1	0.0165(9)
O6	0.2283(4)	1/2	0.6390(4)	1	0.0187(9)
O7	0.1434(4)	1/2	0.2953(4)	1	0.0151(9)
O8	0	1/2	1/2	1	0.055(3)
O9	0.488(2)	1/2	0.6021(18)	0.207(18)	0.026(8)

### PHYSICAL AND OPTICAL PROPERTIES

Vránaite forms intergrowths of subparallel prisms up to 100  $\mu\text{m}$  long (Fig. 3a), which are indistinguishable visually and in backscattered electron images (Fig. 3c) from boralsilite. An indistinct lamellar twinning parallel to  $\{001\}$  was observed optically. Vránaite is brittle and its hardness (Mohs) is 4½. Cleavage and parting were not observed; its fracture is irregular. Density could not be measured because of the paucity of material and because of the intimate intergrowths with associated phases. The calculated density is 2.99  $\text{g/cm}^3$  based on the empirical formula.

Fluorescence bands were observed between 50 and 2500  $\text{cm}^{-1}$  under excitation by 532 nm Nd:YAG and 633 nm He-Ne lasers during Raman spectroscopy measurements.

Vránaite is transparent, colorless, and non-pleochroic with a white streak; its luster is vitreous. It is optically biaxial (–),  $n_{\alpha} = 1.607$  (1),  $n_{\beta} = 1.634$  (1),  $n_{\gamma} = 1.637$  (1) (white light using a spindle stage). The  $2V_x$  was observed to be small, but it could not be measured because of indistinct interference figures and indistinct extinctions in some orientations. The calculated  $2V$  angle is 36.4°. Dispersion could not be observed. The orientation is  $X \approx c$ ;  $Y \approx a$ ;  $Z = b$ .

### CHEMICAL COMPOSITION AND COMPATIBILITY INDEX

To select a composition to represent vránaite, we have used the data in Tables 1 and 2 of Novák et al. (2015), as these analyses were obtained on the section from which the crystals used to obtain the X-ray diffraction and optical data were extracted. However, the LA-ICP-MS  $\text{B}_2\text{O}_3$  contents of vránaite in their Table 2 are higher than the ideal  $\text{B}_2\text{O}_3$  content inferred for vránaite, whereas the EMPA  $\text{B}_2\text{O}_3$  contents in their Table 1 cluster around the ideal vránaite  $\text{B}_2\text{O}_3$  content (Figs. 4 and 5). Consequently, we have used only the EMPA  $\text{B}_2\text{O}_3$  contents to represent vránaite (Table 4). The resulting composition agrees with the composition determined in the crystal structure refinement if Li and Be are assumed to replace Al as the refinement suggests. The analytical total is 99.31 wt%, a more reasonable value than the totals obtained if ICP-MS  $\text{B}_2\text{O}_3$  values are assumed, 100.75–103.45 wt%, or on average 101.96 wt% (Novák et al. 2015).

The empirical formula, calculated on the basis of 24 cations per formula unit is  $(\text{Al}_{14.65}\text{Li}_{1.08}\text{Be}_{0.47}\text{Fe}_{0.02})_{\Sigma 16.22}\text{B}_{3.89}\text{Si}_{3.88}\text{O}_{36.62}$ . The simplified formula, assuming fully occupied B, Si, Al1, Al2,

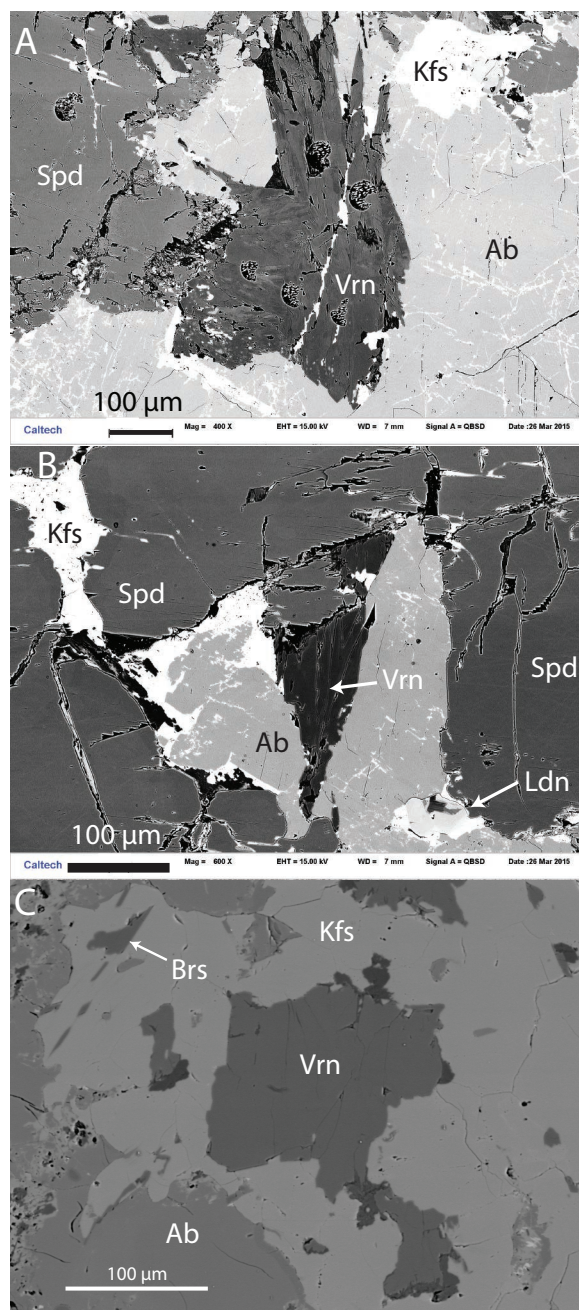


**FIGURE 3.** Backscattered electron images of vránaite (Vrn) in albite (Ab) or K-feldspar (Kfs) and contiguous with spodumene (Spd). (a) Grain 1 showing fibrous appearance revealed by compositional heterogeneity. This grain was used for the X-ray diffraction and optical work. Image taken at Caltech. (b) Grain 2. Bright grain (Ldn) is londonite. Image taken at Caltech. (c) Grain 3 is a bit farther from spodumene. Note that boralsilite (Brs) is separate from vránaite. Image taken at Masaryk University.

and Al3 sites and half-occupied Al4 and Al5 sites (see above), is  $\text{Al}_{16}\text{B}_4\text{Si}_4\text{O}_{38}$ , which corresponds to (in wt%): 68.2  $\text{Al}_2\text{O}_3$ , 11.6  $\text{B}_2\text{O}_3$ , and 20.1  $\text{SiO}_2$ . The Raman spectrum shows no peaks in the range between 3000 and 4000  $\text{cm}^{-1}$  typically attributed to OH

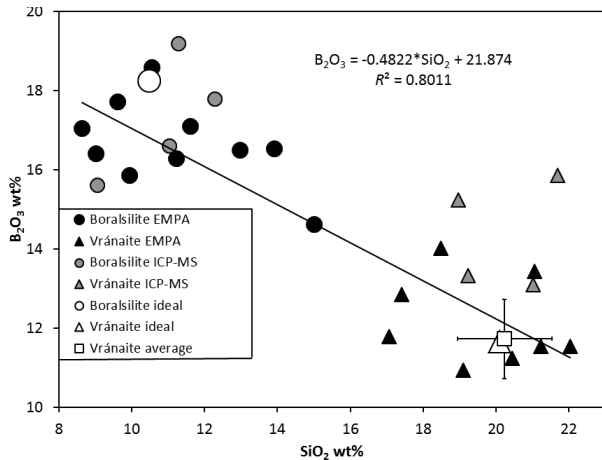


**FIGURE 4.** Plot of  $B_2O_3$  (EMPA and LA-ICP-MS) and  $SiO_2$  (EMPA only) contents (wt%) of boralsilite and vránaite from Novák et al. (2015), Tables 1 and 2 therein. The average composition of vránaite is from Table 4. Trend line is a least-squares fit to the EMPA data.

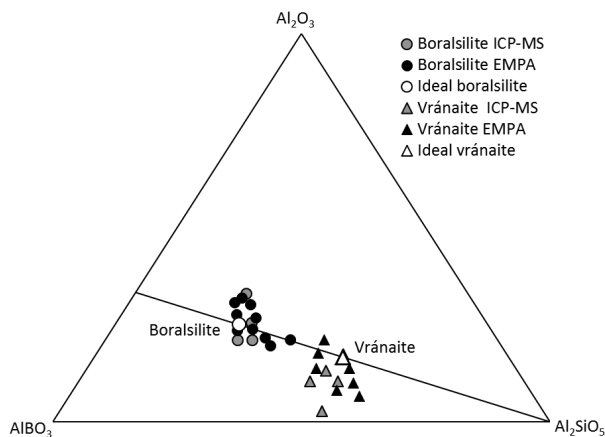


**FIGURE 5.** Compositions of boralsilite and vránaite (Novák et al. 2015) projected from  $Li_2O$  and  $BeO$  onto the  $Al_2O_3$ - $AlBO_3$ - $Al_2SiO_5$  part of the  $Al_2O_3$ - $B_2O_3$ - $SiO_2$  (BAS) system. The symbols distinguish between  $B_2O_3$  contents measured with the electron microprobe (black filled) and with the laser ablation ICP-MS (gray filled).

(Fig. 6), and thus vránaite is formulated as an anhydrous mineral.

The Gladstone-Dale relation (Mandarino 1981) gives a compatibility index  $1 - (K_p/K_c) = 0.001$  (superior).

Novák et al. (2015) showed that both boralsilite and vránaite (“boron mullite”) were compositionally heterogeneous with a minimal gap in miscibility between the two minerals. This compositional variation and gap are evident in Figures 4 and 5.

Vránaite Li contents average six times those of associated boralsilite, which contains the most Li reported in boralsilite to date (Fig. 7). Vránaite is also richer in Be than associated boralsilite.

#### RELATIONS TO OTHER COMPOUNDS: NATURAL AND SYNTHETIC

Vránaite is the third anhydrous ternary  $SiO_2$ - $B_2O_3$ - $Al_2O_3$  mineral, and like the other two, boralsilite and boromullite, it

**TABLE 4.** Analytical data (in wt%) for vránaite

Constituent	Mean	Used	no.	Range	St.dev.	EMPA Std./method
$SiO_2$	20.24	20.24	4	18.98–21.70	1.3	sanidine
$B_2O_3^a$	14.37	–	4	13.09–15.85	1.4	LA-ICP-MS
$B_2O_3^a$	11.73	11.73	5	10.92–13.43	1.0	danburite
$Al_2O_3$	64.77	64.77	4	62.77–65.51	1.3	sanidine
$BeO$	1.03	1.03	4	0.47–1.40	0.40	LA-ICP-MS
$FeO$	0.13	0.13	4	0.08–0.18	0.05	almandine
$MnO$	0.01	0.01	4	bdl–0.03	0.02	spessartine
$Li_2O$	1.40	1.40	4	1.19–1.54	0.15	LA-ICP-MS
$Na_2O$	0.01	–	4	0.01–0.02	0.01	albite
$Na_2O$	bdl	0	4	bdl–bdl	–	LA-ICP-MS
F	0.03	0	4	bdl–0.06	0.03	topaz
Total	–	99.31	–	–	–	–

Note: no. = number of analyses.  $^aB_2O_3$  measured on the same grains. bdl = below detection level. Total includes EMPA  $B_2O_3$  and LA-ICP-MS  $Na_2O$ , but not F, which is assumed to be below detection level. Source: Novák et al. (2015), Tables 1–3.

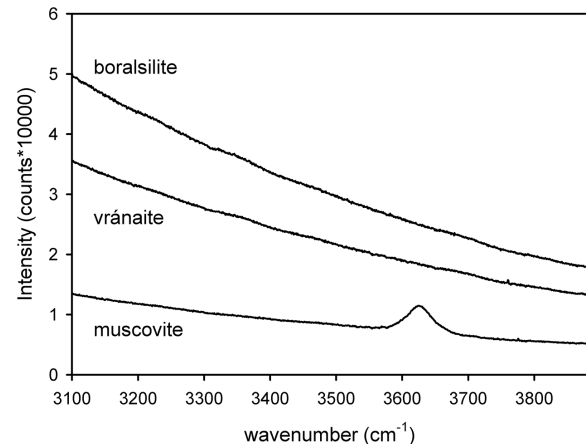


**FIGURE 6.** Raman spectrum of vránaite compared to spectra of boralsilite and muscovite.

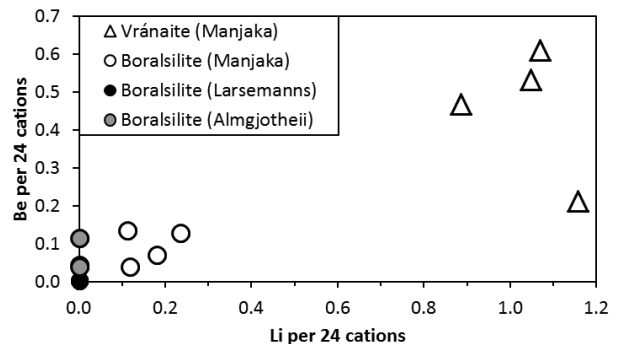


**FIGURE 7.** Plot of Li contents of boralsilite from the Larsemann Hills, Antarctica, and Almgjotheii, Rogaland, Norway (ion microprobe data, Grew et al. 1998), for comparison with data on boralsilite and vránaite from Manjaka (Novák et al. 2015, Table 2; vránaite formulas calculated using ICP-MS  $B_2O_3$  contents). Vránaite contains 1.19–1.54 wt%  $Li_2O$  and 0.47–1.40 wt%  $BeO$ , several times their contents in boralsilite at Manjaka.

belongs to the family of mullite-type boron compounds in the classification of Fischer and Schneider (2008), that is, chains of edge-sharing Al octahedra cross-linked by various polyhedra containing Al, B, and Si. The symmetry of vránaite and boralsilite

can be derived from the orthorhombic supergroup *Pbam* represented by B-doped mullite using a Bärnighausen tree (Fischer and Schneider 2008). Vránaite has an index of 4 lower than mullite (*Pbam* →  $t2 P2/m$  →  $k2 I2/m$ , where *t* = translationgleich and *k* = klassengleich), whereas boralsilite has an index of 8 lower; i.e., the symmetry of vránaite is higher than that of boralsilite (Reinhard Fischer, personal communication, 2016).

Table 5 shows how similar vránaite, boralsilite, and boromullite are to one another. A partial chemical analysis such as EMPA without B<sub>2</sub>O<sub>3</sub> would be needed to unambiguously distinguish them, although 2*V* could give a preliminary indication. X-ray powder diffraction patterns of vránaite (this paper) and boralsilite (Grew et al. 2008) are very similar; positions of the most intense peaks differ only slightly, and intensities are similar. Moreover, both minerals have prismatic crystal habit and therefore preferred crystal orientation in a measured sample may affect measured intensities. Consequently, distinguishing vránaite from boralsilite using only powder X-ray diffraction without EMPA may not be possible.

Boromullite differs from boralsilite and vránaite in that it corresponds to a 1:1 polysome composed of an Al<sub>2</sub>SiO<sub>5</sub> module having the topology and stoichiometry of sillimanite and of an Al<sub>3</sub>BO<sub>9</sub> module that is a type of mullite defect structure (Buick et al. 2008). Vránaite and boralsilite are very similar in structure (Fig. 2). Overall, boralsilite can be considered as a structure in which half of the Si<sub>2</sub>O<sub>7</sub> dimers in vránaite are replaced by two B tetrahedra accompanied by some rearrangement of Al polyhedra. Specifically, the BO<sub>3</sub> triangle in vránaite corresponds to the B<sub>3</sub>O<sub>3</sub> triangle in boralsilite and the partially occupied tetrahedral B site formed when O9 is occupied in vránaite corresponds to the B<sub>2</sub>O<sub>4</sub> tetrahedron in boralsilite. Also, the Al5 site in vránaite corresponds nicely to the Al3 site in boralsilite. A nearly continuous compositional series between vránaite and boralsilite is not surprising given the similarity in the structures, including their geometrical parameters.

A large number of anhydrous, ternary compounds related to

mullite and having orthorhombic symmetry have been synthesized; these have been referred to collectively as “boron mullite” and were thought to occupy a wide field in SiO<sub>2</sub>-B<sub>2</sub>O<sub>3</sub>-Al<sub>2</sub>O<sub>3</sub> space (Fig. 1, e.g., Werding and Schreyer 1992, 1996; Fischer and Schneider 2008; Lührs et al. 2012, 2013, 2014). One such compound was synthesized by Werding and Schreyer (1992), who reported it to have orthorhombic symmetry and the composition Al<sub>16</sub>B<sub>4</sub>Si<sub>4</sub>O<sub>38</sub> based on the Al:Si ratio in the starting gel and a boron analysis. Similarities in the powder X-ray diffraction patterns between this phase, several aluminoborates and sillimanite led Werding and Schreyer (1992) to suggest that all these phases are boron-bearing derivatives of sillimanite. The reported pattern for Al<sub>16</sub>B<sub>4</sub>Si<sub>4</sub>O<sub>38</sub> included a reflection at 20.301° 2θ that required indexing its powder XRD pattern with a supercell having two doubled cell parameters characteristic of sillimanite (Grew et al. 2008). These authors attributed the reflection at 20.301° 2θ to the incipient development of a boralsilite-like structure; and re-indexed its powder XRD pattern with a mullite cell to give cell parameters very similar to those for other “boron-mullites.” This re-interpretation is consistent with the crystal structure refinement by the Rietveld method (Lührs et al. 2014) of a synthetic compound with the composition determined by prompt γ activation analysis, Al<sub>4.19(7)</sub>Si<sub>0.91(6)</sub>B<sub>0.90(2)</sub>O<sub>9.45</sub>, i.e., very close to Al<sub>16</sub>B<sub>4</sub>Si<sub>4</sub>O<sub>38</sub>. The compound has orthorhombic symmetry, space group, *Pbam*: *a* = 7.508466(1), *b* = 7.651508(1), *c* = 2.832082(7) Å, that is, mullite-like (Lührs et al. 2014), and distinct from vránaite.

Analyses of “boron-mullites” give linear arrays radiating from Al<sub>5</sub>BO<sub>9</sub> (Figs. 1 and 8) in lieu of a broad area of compositions in the SiO<sub>2</sub>-B<sub>2</sub>O<sub>3</sub>-Al<sub>2</sub>O<sub>3</sub> system, that is, “boron-mullites” between 3:2 mullite and Al<sub>5</sub>BO<sub>9</sub> (Lührs et al. 2014); boromullite and several synthetic compounds between sillimanite and Al<sub>3</sub>BO<sub>5</sub> (Buick et al. 2008), and “boron-mullites” between Al<sub>16</sub>B<sub>4</sub>Si<sub>4</sub>O<sub>38</sub> and Al<sub>5</sub>BO<sub>9</sub> (Grew et al. 2008).

Not all synthetic anhydrous ternary phases in the “boron-mullite” field of the SiO<sub>2</sub>-B<sub>2</sub>O<sub>3</sub>-Al<sub>2</sub>O<sub>3</sub> system are “boron-mullite.” Grew et al. (2008) distinguished synthetic disordered boralsilite from “boron-mullite” since its X-ray diffraction pattern resembled that of boralsilite, but differed from that of ordered boralsilite in that reflections were broadened and their intensities modified. These differences could result from either a very small size of coherently scattering domains or strain associated with lattice imperfections (Grew et al. 2008). These authors interpreted the presence of a low “hump” between 20.0 and 20.4° 2θ, like the weak reflection at 20.301° 2θ in orthorhombic Al<sub>16</sub>B<sub>4</sub>Si<sub>4</sub>O<sub>38</sub>, to represent the incipient conversion of “boron-mullite” to a “boralsilite-like” structure, i.e., a structure like either boralsilite or vránaite. In marked contrast to “boron-mullite,” compositional variation in disordered boralsilite followed a linear trend at high angles to the linear arrays for “boron mullite” and come close to intersecting the boralsilite-vránaite join (Fig. 8), i.e., the disordered phase could be just as well be called “disordered” vránaite.

## OCCURRENCE AND ORIGIN

Vránaite occurs in the Manjaka pegmatite, one of the granitic pegmatites in the Sahatany Valley pegmatite field, located about 25 km SW of the town Antsirabe in the northeast part of the Itremo Region, Central Madagascar (Novák et al. 2015).

**TABLE 5.** Comparison of vránaite to related minerals

Mineral	Vránaite	Boralsilite	Boromullite	Sillimanite
Formula	Al <sub>16</sub> B <sub>4</sub> Si <sub>4</sub> O <sub>38</sub>	Al <sub>16</sub> B <sub>8</sub> Si <sub>2</sub> O <sub>37</sub>	Al <sub>9</sub> BSi <sub>2</sub> O <sub>19</sub>	Al <sub>2</sub> SiO <sub>5</sub>
Crystal system	monoclinic	monoclinic	orthorhombic	orthorhombic
Space group	<i>I</i> 2/ <i>m</i>	<i>C</i> 2/ <i>m</i>	<i>C</i> mc2 <sub>1</sub>	<i>P</i> bnm
Z	1	2	2	4
<i>a</i> (Å)	10.383(1)	14.767(1)	5.717(2)	7.4841(1)
<i>b</i> (Å)	5.6682(7)	5.574(1)	15.023(5)	7.6720(3)
<i>c</i> (Å)	10.823(1)	15.079(1)	7.675(3)	5.7707(2)
β (°)	90.11(1)	91.96(1)	90.00	90.00
<i>V</i> (Å <sup>3</sup> )	636.97(13)	1240.4(2)	659.2(7)	331.34(1)
<i>n</i> <sub>α</sub>	1.607(1)	1.629(1)	1.627(1)	1.653–1.661
<i>n</i> <sub>β</sub>	1.634(1)	1.640(1)	1.634(1)	1.657–1.662
<i>n</i> <sub>γ</sub>	1.637(1)	1.654(1)	1.649(1)	1.672–1.683
2 <i>V</i> <sub>x</sub> (°)	36.4	98.2(6)	123(2)	150–159
Orientation	Z = <b>b</b>	Z = <b>b</b>	–	Z = <b>c</b>
Cleavage	none	fair	none	perfect
Powder XRD, <i>d</i> <sub>obs</sub> (Å), <i>I</i>	5.40, 96 5.19, 99 4.97, 74 3.658, 75 3.403, 100 2.496, 61 2.171, 75 1.5183, 61	5.36, 70 5.19, 100 4.95, 60 4.31, 70 3.378, 60 2.162, 40	5.37, 50 3.38, 100 2.67, 60 2.51, 60 2.19, 80 1.512, 80	5.36, 16 3.42, 100 3.37, 65 2.204, 60 2.541, 40 2.679, 30 2.111, 20
Reference	1	2, 3	4	5, 6

Notes: 1 = this study; 2 = Grew et al. (1998); 3 = Peacor et al. (1999); 4 = Buick et al. (2008); 5 = Anthony et al. (2003); 6 = Bish and Burnham (1992).

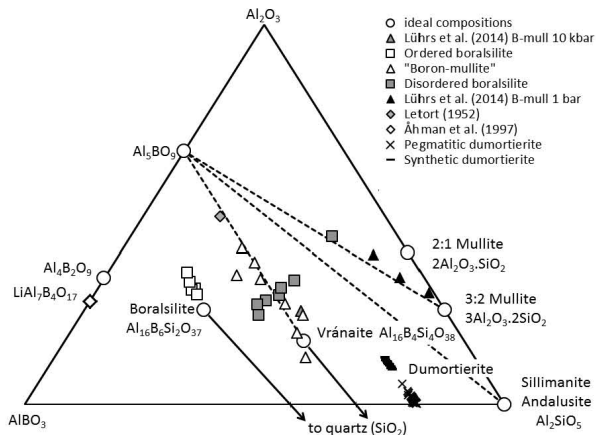


**FIGURE 8.** Phases related to mullite, together with dumortierite, plotted in the  $\text{Al}_2\text{O}_3$ - $\text{AlBO}_3$ - $\text{Al}_2\text{SiO}_5$  part of the  $\text{Al}_2\text{O}_3$ - $\text{B}_2\text{O}_3$ - $\text{SiO}_2$  (BAS) system, with  $\text{LiAl}_7\text{B}_4\text{O}_{17}$  projected from  $\text{Li}_2\text{O}$ . Dashed lines mark the linear areas of compositions radiating from  $\text{Al}_3\text{BO}_3$ . The arrows are tie lines from boralsilite and vránaite to quartz, which plots off the diagram. Sources of data in addition to references cited in the legend: pegmatitic dumortierite containing more  $\text{Al}_2\text{O}_3$  than the  $\text{AlBO}_3$ - $\text{Al}_2\text{SiO}_5$  join (Cempírek 2003; Cempírek and Novák 2005; Cempírek et al. 2010; Wadoski et al. 2011); dumortierite synthesized at 650–700 °C, 3–5 kbar (Werdning and Schreyer 1990); and “boron-mullite,” ordered boralsilite and disordered boralsilite (Grew et al. 2008).

Coordinates in WGS84 (latitude, longitude): 20°04'35" S, 46°57'09" E. Vránaite is in contact with spodumene (Figs. 3a and 3b), K-feldspar (Fig. 3b and 3c), albite, and a secondary Al-rich clay mineral. Boralsilite also occurs in this association, although separately from vránaite, the closest approach being 100  $\mu\text{m}$  (Fig. 3c). Zoned tourmaline 1 (elbaite to fluor-elbaite), zoned londonite-rhodizite, quartz, and beryl are also associated with spodumene, but none of these minerals contacts vránaite. Although the primary assemblage of spodumene + K-feldspar + albite contains minor quartz, vránaite, and boralsilite are part of a later assemblage with albite that is quartz-undersaturated.

Boralsilite and vránaite are inferred to have grown under conditions far from equilibrium resulting from a combined pressure + chemical quenching in the Manjaka pegmatite. We attribute origin of boralsilite and vránaite to a liquid rich in alkalis, Be, and B, and to having high  $a(\text{CO}_2)$  together with low  $a(\text{H}_2\text{O})$  due to early melt contamination by carbonate in the host rocks. The unusual fluid composition is indicated by the low abundance of hydrous phases, presence of secondary rhodochrosite and minor extent of exocontact reactions adjacent to the pegmatite. Novák et al. (2015) estimated the temperature-pressure conditions for crystallization of boralsilite and vránaite to be ~350–450 °C and ~2–3 kbar (Fig. 9), i.e., very late solidus or early subsolidus conditions that later graded into crystallization of rhodizite-londonite.

## DISCUSSION

Ternary phases (either anhydrous or hydrous) in the  $\text{SiO}_2$ - $\text{B}_2\text{O}_3$ - $\text{Al}_2\text{O}_3$  (BAS) system (Fig. 1) are relatively rare in pegmatites; instead, boron is largely tied up in species of the tourmaline supergroup, and the Manjaka pegmatite is no excep-

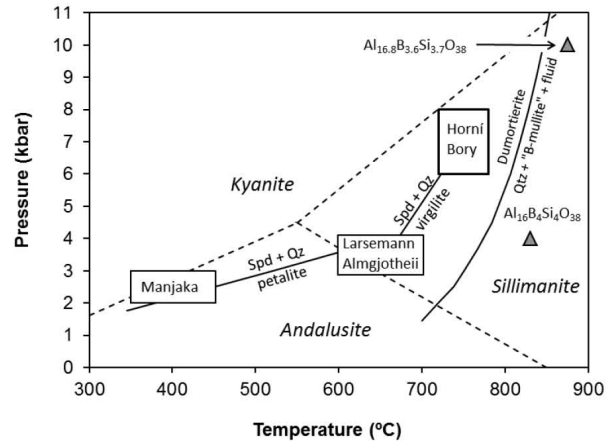


**FIGURE 9.** Pressure-temperature diagram for boralsilite crystallization (rectangles) in the Larsemann Hills, Antarctica, and Almgjotheii, Norway (Grew et al. 2008), Horni Bory, Czech Republic (Cempírek et al. 2010), and Manjaka, Madagascar (Novák et al. 2015; this paper), and for “boron-mullite” ( $\text{Al}_{16}\text{B}_4\text{Si}_4\text{O}_{38}$ , Werdning and Schreyer 1992;  $\text{Al}_{16.8}\text{B}_{3.6}\text{Si}_{3.7}\text{O}_{38}$ , Lührs et al. 2014). Source for experimental data:  $\text{Al}_2\text{SiO}_5$  polymorphs (italics and dashed lines, Pattison 1992), dumortierite breakdown (Werdning and Schreyer 1996), breakdown of spodumene + quartz (Spd + Qtz, London 1984).

tion. The dumortierite supergroup (Pieccka et al. 2013) is found in a fair number of pegmatites, although much less abundantly than tourmaline. In contrast, boralsilite is known only from four localities worldwide (Grew et al. 1998, 2008; Cempírek et al. 2010; Novák et al. 2015), and vránaite so far from only one locality. Compositions of boralsilite, vránaite, and Al-rich dumortierite (higher Al/Si ratio than the end-member  $\text{Al}_7\text{BSi}_3\text{O}_{18}$ ) containing little Ti, Fe, Mg, As, and Sb projected from  $\text{H}_2\text{O}$  and other non-BAS constituents plot in the  $\text{Al}_2\text{O}_3$ -dominant third of the  $\text{SiO}_2$ - $\text{B}_2\text{O}_3$ - $\text{Al}_2\text{O}_3$  plane ( $\text{Al}_2\text{SiO}_5$ - $\text{AlBO}_3$ - $\text{Al}_2\text{O}_3$ , Fig. 8). Compositions of dumortierite from pegmatites in the Czech Republic (Cempírek 2003), as well as dumortierite associated with boralsilite, approach that of the ideal anhydrous end-member when projected onto the  $\text{Al}_2\text{SiO}_5$ - $\text{AlBO}_3$ - $\text{Al}_2\text{O}_3$  plane.

In a review of the two original localities of boralsilite (Larsemann Hills, Antarctica; Almgjotheii, Norway), Grew et al. (2008) concluded that a combination of a B-rich source and relatively low water content, together with limited fractionation, resulted in an unusual buildup of B, but not of Li, Be, and other elements normally concentrated in pegmatites. The resulting conditions are favorable for precipitation of boralsilite instead of elbaite, which is often formed in more fractionated pegmatites. An important consideration is the amount of water in the melt: if the residual fluids were drier, there would have been less opportunity for metasomatic loss of B from the pegmatite to the host rock, a process that often depletes pegmatites in B (London et al. 1996). Grew et al. (2008) also noted the common association of boralsilite with graphic tourmaline-quartz intergrowths in the Larsemann Hills; these intergrowths could be the products of rapid crystallization due to oversaturation in tourmaline. London et al. (1996) attributed similar graphic intergrowths of tourmaline and quartz from the Belo Horizonte 1 pegmatite, California, to oversaturation. Rapid growth of

tourmaline and quartz could have left a residual melt or fluid thoroughly depleted in Fe and Mg; less so in B. However, such graphic intergrowths have not been found at Almgjotheii or at the other two world localities for boralsilite, Horní Bory, Czech Republic, and Manjaka. A boron-rich source rock was not found in the immediate vicinity of the boralsilite-bearing veinlets at Almgjotheii or Horní Bory, but more distant rocks of the Gföhl Unit could have been the source of B for the Horní Bory veinlet (Cempírek et al. 2010). These authors reported that intrusion of the boralsilite-bearing veinlet at Horní Bory post-dated foliation in the host granulite and suggested the veinlet is a product of decompressional melting processes. Boralsilite most likely crystallized in a H<sub>2</sub>O-poor system. In contrast to the Larsemann Hills and Almgjotheii, there is evidence for some concentration of Li in the Horní Bory veinlet (Cempírek et al. 2010). Despite the striking differences with the other three localities, notably the much lower temperature of crystallization and Li enrichment indicated by the association with spodumene, the Manjaka pegmatite shares several features with them: little loss of boron to the host rock and possible decompression suggested by the presence of spodumene + quartz intergrowths. Such intergrowths (SQI) are attributed in other pegmatites to petalite breakdown (e.g., Tanco in Manitoba, Canada, London 2008), which implies for Manjaka decompression to form petalite from primary spodumene + quartz, followed by isobaric cooling during which petalite broke down entirely to a second generation of spodumene + quartz. There is an alternative scenario consistent with observed textures and mineral assemblages and not involving an incursion into the petalite stability field, namely, a chemical quench during cooling or decompression within the spodumene + quartz stability field and resulting in sudden saturation in quartz, possibly from loss of alkalis to the fluid phase, and rapid precipitation of spodumene as SQI.

Although the breakdown curve for dumortierite shown in Figure 9 does not represent a univariant reaction in the SiO<sub>2</sub>-B<sub>2</sub>O<sub>3</sub>-Al<sub>2</sub>O<sub>3</sub>-H<sub>2</sub>O system, it is strongly suggestive that dumortierite is a stable ternary SiO<sub>2</sub>-B<sub>2</sub>O<sub>3</sub>-Al<sub>2</sub>O<sub>3</sub> phase with quartz present up to 700–830 °C at  $P < 8$  (Werdning and Schreyer 1992, 1996), which is consistent with its widespread occurrence in metamorphic rocks (Grew 1996). Less evident is whether a second BAS phase such as “boron-mullite,” boralsilite, or vránaite, could be stable in addition to or instead of dumortierite, particularly in compositions richer in Al<sub>2</sub>O<sub>3</sub> or B<sub>2</sub>O<sub>3</sub> as only synthesis data are available on these minerals. Synthesis of a “boron mullite” has been reported at  $P$ - $T$  conditions within the dumortierite stability field (500–800 °C, 2–10 kbar, Werdning and Schreyer 1984, 1996; Wodara and Schreyer 2001), but this material was not well characterized. Only “boron mullite” synthesized at temperatures above dumortierite breakdown (Fig. 9) has been shown to have a mullite structure by detailed X-ray diffraction study, e.g., 750–800 °C, 1–2 kbar, Grew et al. 2008; 875 °C, 10 kbar, Lührs et al. 2014). In contrast, X-ray diffraction has confirmed the synthesis of disordered and ordered boralsilite at temperatures both within the dumortierite stability field and above the curve for dumortierite breakdown (Pöter et al. 1998; Grew et al. 2008). It is thus possible that Werdning and Schreyer (1984, 1996) and Wodara and Schreyer (2001) mistook disordered and ordered boralsilite for “boron

mullite,” and, as a result, there is reason to believe “boron-mullite” is stable only at temperatures above the breakdown of dumortierite at pressures up to at least 10 kbar (Grew et al. 2008; Lührs et al. 2014).

Grew et al. (2008) were not successful in identifying what physical-chemical conditions favor transformation of disordered to ordered boralsilite. No evidence was found that duration, gel composition, proportion of H<sub>3</sub>BO<sub>3</sub> or seeding with ordered boralsilite played a critical role. That some experimental runs containing an apparently amorphous phase yielded ordered boralsilite suggests that chance seeding by an unknown impurity could play a role.

Natural boralsilite at all four localities crystallized in the stability field of dumortierite + quartz (Fig. 9). Boralsilite at Manjaka crystallized in the absence of quartz, but at temperatures so much below the temperature of dumortierite breakdown that silica undersaturation is not a plausible explanation for the presence of boralsilite and vránaite and absence of dumortierite in the Manjaka pegmatite. More plausible is the stabilization of vránaite in addition to boralsilite by the presence of significant Li in vránaite (Fig. 7), whereas boralsilite Li contents seem too low to explain its appearance in the Manjaka pegmatite.

Crystallization of boralsilite and vránaite has analogies with that reported for metastable crystallization of cristobalite in crystal-rich fluid inclusions hosted in spodumene in Jiajika pegmatite deposit, China (Li and Chou 2015). These authors attributed the formation of cristobalite to a 1.5–2.4 kbar decrease in pressure inside the inclusions and extension of the cristobalite stability field to lower temperatures by Li and H<sub>2</sub>O.

There are two possible scenarios for the crystallization of boralsilite and vránaite.

(1) A B- and Al-rich bulk composition favored stable crystallization of boralsilite over dumortierite, even in the presence of quartz at sufficiently high temperatures; additionally isolation from quartz by albite and an assist from Li could have stabilized boralsilite and vránaite at much lower temperatures in the Manjaka pegmatite. Dumortierite is present in pegmatites at three of the four localities for boralsilite (Manjaka is the exception), but interpretation of its relationship with boralsilite is complicated by microstructural evidence for two generations (e.g., Larsemann Hills, Wadoski et al. 2011) and by the variable presence of Ti, Fe, Mg, As, or Sb (Grew et al. 1998; Wadoski et al. 2011; Cempírek et al. 2010), i.e., these impurities, where present in significant amounts, could have stabilized dumortierite in addition to boralsilite. Nonetheless, even dumortierite containing relatively low concentrations of these impurities does not block tie lines from quartz to either vránaite or boralsilite (arrows) in the Al<sub>2</sub>SiO<sub>5</sub>-AlBO<sub>3</sub>-Al<sub>2</sub>O<sub>3</sub> plane (Fig. 8), which is consistent with higher boron concentrations stabilizing boralsilite or vránaite instead of dumortierite.

(2) Boralsilite and vránaite crystallized metastably instead of dumortierite due to their relative structural simplicity, that is, the system follows the path of metastable crystallization described by the Ostwald principle and the Goldsmith's (1953) “simplicity” rule, which states that, in the Ostwald cascade of phase transformations, phases with higher “simplicity” (lower complexity) crystallize first even if they are unstable from the energetic point of view. Numerical estimates of structural

**TABLE 6.** Structural complexity of selected aluminoborosilicates

Mineral	Chemical formula (average)	$v$ , atoms	$I_G$ (bits/atom)	$I_{G, \text{total}}$ (bits/cell)	References
"boron-mullite"	$\text{Al}_{16.8}\text{B}_{3.6}\text{Si}_{3.7}\text{O}_{38}$	16	2.250	36.000	Lührs et al. (2014)
"boron-mullite"	$\text{LiAl}_7\text{B}_4\text{O}_{17}$	29	2.651	76.881	Åhman et al. (1997)
vřánaite	$\text{Al}_6\text{Si}_2\text{B}_2\text{O}_{19}$	34	3.911	132.974	this work
boralsilite	$\text{Al}_{16}\text{Si}_3\text{B}_6\text{O}_{37}$	61	4.619	281.775	Peacor et al. (1999)
dumortierite	$\text{Al}_7\text{Si}_3\text{BO}_{18}$	116	4.099	475.526	Fuchs et al. (2005)

complexity, which were derived by applying Shannon information theory, provided quantitative support to Goldsmith's rule (Krivovichev 2012, 2013). Since structural complexity represents a negative contribution to the total entropy of a crystalline solid (through its configurational part, Krivovichev 2016), crystallization of a metastable phase is entropy driven and governed by kinetics of the process, which favor crystallization of phases with higher configurational entropy first. In the case of the system under consideration, a possible sequence of phase transformations is:

silicate "boron-mullite"  $\rightarrow$  disordered boralsilite  
 $\rightarrow$  ordered boralsilite.

There could be an analogous sequence:

silicate "boron-mullite"  $\rightarrow$  disordered vřánaite  
 $\rightarrow$  ordered vřánaite.

In both cases, crystallization starts with a low-complexity phase and ends with a higher-complexity phase, but not with the most complex phase in the system, which is the stable phase dumortierite (Table 6). Therefore, the occurrence of vřánaite at Manjaka pegmatite may be explained by its crystallization under conditions far from equilibrium and the very specific kinetic regime of quenching. This hypothesis also explains the relative rarity of vřánaite, as crystallization proceeds to the most stable phase, i.e., dumortierite, at most other localities. Given the inverse relationship between structural complexity and configurational entropy (Krivovichev 2016), it seems plausible that disordered boralsilite and vřánaite are less complex than the corresponding ordered phases, but still more complex than silicate "boron-mullite." Compositions plotted in Figure 8 suggest that the succession to form ordered vřánaite would be not overly far from isochemical, whereas additional  $\text{AlBO}_3$  and  $\text{Al}_2\text{O}_3$  are needed to form ordered boralsilite from "boron-mullite." However, the latter sequence cannot be ruled out for this reason alone, because it is likely that "boron-mullite" and disordered boralsilite have a wider range of composition than that reported by Grew et al. (2008) and shown in Figure 8. We have included the boron mullite  $\text{LiAl}_7\text{B}_4\text{O}_{17}$  in Figure 8 to show that Li, an element not generally encountered in mullite, could be present as a subordinate constituent in the "boron-mullite" precursor, and thus scenario (2) is relevant for the Li-bearing system at Manjaka.

Černý (2000) and London (2008) suggested that both pressure and chemical quenches play important roles in the formation of miarolitic cavities, and similar quenches, for example, abrupt change in chemical composition by crystallization of tourmaline + quartz in the Larsemann Hills (or grandidierite at Horní Bory, Cempírek et al. 2010), could have favored metastable crystal-

lization of the mullite precursors to boralsilite and vřánaite. On the other hand, the Manjaka pegmatite containing boralsilite and vřánaite was subject to system opening (Novák et al. 2015), and thus metastable crystallization due to rapid pressure decrease is very likely. Given all these opportunities for metastable crystallization, we tend to favor the second scenario, in which some mix of a pressure and chemical quench resulted in conditions favorable to metastable crystallization of disordered "boron-mullite" that subsequently recrystallized into ordered boralsilite and vřánaite.

## IMPLICATIONS

Vřánaite is the third nominally ternary  $\text{B}_2\text{O}_3$ - $\text{Al}_2\text{O}_3$ - $\text{SiO}_2$  phase in the mullite-type family of structures to be discovered in nature, the others being boralsilite and boromullite. A greater variety of these mullite-like  $\text{B}_2\text{O}_3$ - $\text{Al}_2\text{O}_3$ - $\text{SiO}_2$  phases have been synthesized and studied in detail because of their many potential applications, notably Al borates such as  $\text{Al}_5\text{BO}_9$ , in optical electronics, structure applications, and tribology—e.g., refractory linings because of their high resistance to corrosion, optically translucent ceramics for high-temperature furnace windows, and linings in nuclear plants because of their capability of absorbing neutrons (Fischer and Schneider 2008; Gatta et al. 2010, 2013 and references cited therein). Most synthetics appear to be B-bearing mullite, and it remains an open question whether any correspond to boromullite, a polysome composed of  $\text{Al}_5\text{BO}_9$  and sillimanite modules (Buick et al. 2008). Analogs of boralsilite are relatively difficult to synthesize (Pöter et al. 1998; Grew et al. 2008); "boron-mullite" and disordered boralsilite crystallize more readily. The syntheses and the natural occurrences suggest that crystallization of boralsilite and vřánaite is a disequilibrium process, beginning with the metastable crystallization of B-bearing mullite and succession by Ostwald step rule to ordered boralsilite and vřánaite, but not always reaching dumortierite, the stable phase under the conditions at which pegmatites crystallized. The presence of metastable phases is consistent with increasing evidence for disequilibrium processes in pegmatites, in which high viscosity that slows the movement of constituents, supercooling, and quenches associated with rapid changes in composition or pressure play important roles (Černý 2000; London 2008, 2014).

Disequilibrium conditions in Li, Be, B-rich systems could be also achieved by metamorphic overprint of fractionated systems. For example, metamorphosed pegmatite veins at Virorco, Argentina (Galliski et al. 2012) evidence remobilization of Li, Be, and B, resulting in secondary tourmaline, chrysoberyl, dumortierite, and holtite. In a situation where the  $\text{H}_2\text{O}$ -depletion at the end of secondary crystallization was accompanied by  $\text{B}_2\text{O}_3$  activities approaching saturation, anhydrous borosilicates might form instead of dumortierite.

## ACKNOWLEDGMENTS

We thank Reinhard Fischer, Alessandro Gastoni, and the Technical Editor for their thoughtful reviews of the manuscript, and we thank members of the IMA CNMNC for constructive comments on the proposal submitted to the Commission for approval. This work was supported by the research project GAČR P210/14/13347S (J.C., M.N., P.G., R.Š., M.V.G.). SEM and EBSD analyses were carried out at the Caltech GPS Division Analytical Facility, which is supported, in part, by NSF Grants EAR-0318518 and DMR-0080065. A portion of this study was funded by the John Jago Trelawney Endowment to the Mineral Sciences Department of the Natural History Museum of Los Angeles County. L.A.G. acknowledges the support of a Discovery Grant from the Natural Sciences and Engineering Research Council of Canada. S.V.K. was supported in this work by the Russian Foundation for Basic Research (grant 16-05-00293).

## REFERENCES CITED

- Åhman, J., Svensson, G., and Grins, J. (1997) Lithium aluminium borate,  $\text{LiAl}_3\text{B}_3\text{O}_{17}$ . *Acta Chemica Scandinavica*, 51, 1045–1050.
- Anthony, J.W., Bideaux, R.A., Bladh, K.W., and Nichols, M.C., Eds. (2003) *Handbook of Mineralogy*, vol. II. Mineralogical Society of America, Chantilly, Virginia.
- Bish, D.L., and Burnham, C.W. (1992) Rietveld refinement of the crystal structure of fibrolitic sillimanite using neutron powder diffraction data. *American Mineralogist*, 77, 374–379.
- Buick, I., Grew, E.S., Armbruster, T., Medenbach, O., Yates, M.G., Bebout, G.E., and Clarke, G.L. (2008) Boromullite,  $\text{Al}_3\text{BSi}_2\text{O}_{19}$ , a new mineral from granulite-facies metapelites, Mount Stafford, central Australia and a natural analogue of a “boron-mullite.” *European Journal of Mineralogy*, 20, 935–950.
- Burla, M.C., Caliendo, R., Camalli, M., Carrozzini, B., Cascarano, G.L., Giacovazzo, C., Mallamo, M., Mazzzone, A., Polidori, G., and Spagna, R. (2012) SIR2011: a new package for crystal structure determination and refinement. *Journal of Applied Crystallography*, 45, 357–361.
- Cempírek, J. (2003) Mineral associations and chemical composition of dumortierite in granitic pegmatites. M.S. Diplomová práce, Masaryk University, Brno (in Czech).
- Cempírek, J., and Novák, M. (2005) A green dumortierite from Kutná Hora, Moldanubicum, Czech Republic: spectroscopic and structural study. *Crystallization Processes in Granitic Pegmatites*, Elba, Italy, 4–5.
- Cempírek, J., Novák, M., Dolníček, Z., Kotková, J., and Škoda, R. (2010) Crystal chemistry and origin of grandierite, omineleite, boralsilite, and werdingite from the Bory Granulite Massif, Czech Republic. *American Mineralogist*, 95, 1533–1547.
- Cempírek, J., Grew, E.S., Kampf, A.R., Ma, C., Novák, M., Gadas, P., Škoda, R., Vašíňová-Galiová, M., Pezzotta, F., and Groat, L.A. (2016) Vránaite, IMA 2015-084. CNMNC Newsletter No. 29, February 2016, page 200; *Mineralogical Magazine*, 80, 199–205.
- Černý, P. (2000) Constitution, petrology, affiliations and categories of miarolitic pegmatites. *Memoire della Società Italiana di Scienze Naturali e dei Musei Civici di Storia Naturale di Milano*, 30, 5–12.
- Fischer, R.X., and Schneider, H. (2008) Crystal chemistry of borates and borosilicates with mullite-type structures: a review. *European Journal of Mineralogy*, 20, 917–933.
- Fuchs, Y., Ertl, A., Hughes, J.M., Prowatke, S., Brandstaetter, F., and Schuster, R. (2005) Dumortierite from the Gfoehl unit, lower Austria: chemistry, structure and infra-red spectroscopy. *European Journal of Mineralogy*, 17, 173–183.
- Galliski, M.A., Márquez-Zavalía, M.F., Lira, R., Cempírek, J., and Škoda, R. (2012) Mineralogy and origin of the dumortierite-bearing pegmatites of Virocor, San Luis, Argentina. *Canadian Mineralogist*, 50, 873–894.
- Gatta, G.D., Rotiroli, N., Fisch, M., and Armbruster, T. (2010) Stability at high pressure, elastic behavior and pressure-induced structural evolution of “ $\text{Al}_3\text{BO}_6$ ,” a mullite-type ceramic material. *Physics and Chemistry of Minerals*, 37, 227–236.
- Gatta, G.D., Lotti, P., Merlini, M., Liermann, H.-P., and Fisch, M. (2013) High-pressure behavior and phase stability of  $\text{Al}_3\text{BO}_6$ , a mullite-type ceramic material. *Journal of the American Ceramic Society*, 96, 2583–2592.
- Goldsmith, J.R. (1953) A “simplicity principle” and its relation to “ease” of crystallization. *Journal of Geology*, 61, 439–451.
- Grew, E.S. (1996) Borosilicates (exclusive of tourmaline) and boron in rock-forming minerals in metamorphic environments. In E.S. Grew and L.M. Anovitz, Eds., *Boron: Mineralogy, Petrology and Geochemistry*, 33, p. 387–502. Reviews in Mineralogy, Mineralogical Society of America, Chantilly, Virginia.
- Grew, E.S., McGee, J.J., Yates, M.G., Peacor, D.R., Rouse, R.C., Huijsmans, J.P.P., Shearer, C.K., Wiedenbeck, M., Thost, D.E., and Su, S.-C. (1998) Boralsilite ( $\text{Al}_{16}\text{B}_6\text{Si}_3\text{O}_{37}$ ): A new mineral related to sillimanite from pegmatites in granulite-facies rocks. *American Mineralogist*, 83, 638–651.
- Grew, E.S., Graetsch, H., Pöter, B., Yates, M.G., Buick, I., Bernhardt, H.-J., Schreyer, W., Werdning, G., Carson, C.J., and Clarke, G.L. (2008) Boralsilite,  $\text{Al}_{16}\text{B}_6\text{Si}_3\text{O}_{37}$ , and “boron-mullite”: Compositional variations and associated phases in experiment and nature. *American Mineralogist*, 93, 283–299.
- Higashi, T. (2001) ABCOR. Rigaku Corporation, Tokyo.
- Krivovichev, S.V. (2012) Topological complexity of crystal structures: quantitative approach. *Acta Crystallographica*, A68, 393–398.
- (2013) Structural complexity of minerals: information storage and processing in the mineral world. *Mineralogical Magazine*, 77, 275–326.
- (2016) Structural complexity and configurational entropy of crystals. *Acta Crystallographica*, B72, 274–276.
- Letort, Y. (1952) Contribution à l'étude de la synthèse de la mullite. *Transactions of the International Ceramic Congress*, 19–32.
- Li, J., and Chou, I.-M. (2015) An occurrence of metastable cristobalite in spodumene-hosted crystal-rich inclusions from Jiayika pegmatite deposit, China. *Journal of Geochemical Exploration*, <http://dx.doi.org/10.1016/j.gexplo.2015.10.012>.
- London, D. (1984) Experimental phase equilibria in the system  $\text{LiAlSiO}_4\text{-SiO}_2\text{-H}_2\text{O}$ : A petrogenetic grid for lithium-rich pegmatites. *American Mineralogist*, 69, 995–1004.
- (2008) *Pegmatites*. Special Publications. Canadian Mineralogist, 10, 1–347.
- (2014) A petrologic assessment of internal zonation in granitic pegmatites. *Lithos*, 184–187, 74–104.
- London, D., Morgan, G.B. IV, and Wolf, M.B. (1996) Boron in granitic rocks and their contact aureoles. In E.S. Grew and L.M. Anovitz, Eds., *Boron: Mineralogy, Petrology and Geochemistry*, 33, p. 299–330. Reviews in Mineralogy, Mineralogical Society of America, Chantilly, Virginia.
- Lührs, H., Fischer, R.X., and Schneider, H. (2012) Boron mullite: Formation and basic characterization. *Materials Research Bulletin*, 47, 4031–4042.
- Lührs, H., Senyshyn, A., King, S.P., Hanna, J.V., Schneider, H., and Fischer, R.X. (2013) Neutron diffraction and  $^{11}\text{B}$  solid state NMR studies of the crystal structure of B-doped mullite. *Zeitschrift für Kristallographie*, 228, 457–466.
- Lührs, H., Soellradl, S., King, S.P., Hanna, J.V., Konzett, J., Fischer, R.X., and Schneider, H. (2014) Ambient and high-pressure synthesis, composition, and crystal structure of B-mullites. *Crystal Research and Technology*, 49, 21–31.
- Ma, C., and Rossman, G.R. (2008) Barioperovskite,  $\text{BaTiO}_3$ , a new mineral from the Benitoite Mine, California. *American Mineralogist*, 93, 154–157.
- (2009) Tistarite,  $\text{Ti}_2\text{O}_3$ , a new refractory mineral from the Allende meteorite. *American Mineralogist*, 94, 841–844.
- Mandarino, J.A. (1981) The Gladstone-Dale relationship: Part IV. The compatibility concept and its application. *Canadian Mineralogist*, 19, 441–450.
- McGee, J.J., and Anovitz, L.M. (1996) Electron probe microanalysis of geologic materials for boron. In E.S. Grew and L.M. Anovitz, Eds., *Boron: Mineralogy, Petrology, and Geochemistry*, 33, p. 771–788 (second printing 2002). Reviews in Mineralogy, Mineralogical Society of America, Chantilly, Virginia.
- Merlet, C. (1994) An accurate computer correction program for quantitative electron-probe microanalysis. *Mikrochimica Acta*, 114, 363–376.
- Niven, M.L., Waters, D.J., and Moore, J.M. (1991) The crystal structure of werdingite,  $(\text{Mg,Fe})_2\text{Al}_2(\text{Al,Fe})_2\text{Si}_4(\text{B,Al})_2\text{O}_{37}$ , and its relationship to sillimanite, mullite, and grandierite. *American Mineralogist*, 76, 246–256.
- Novák, M., Cempírek, J., Gadas, P., Škoda, R., Vašíňová-Galiová, M., Pezzotta, F., and Groat, L.A. (2015) Boralsilite and Li,Be-bearing “boron mullite”  $\text{Al}_6\text{B}_2\text{Si}_2\text{O}_{19}$ , breakdown products of spodumene from the Manjaka pegmatite, Sahatany Valley, Madagascar. *Canadian Mineralogist*, 53, 357–374.
- Pattison, D.R.M. (1992) Stability of andalusite and sillimanite and the  $\text{Al}_2\text{SiO}_5$  triple point: Constraints from the Ballachulish aureole, Scotland. *Journal of Geology*, 100, 423–446.
- Peacor, D.R., Rouse, R.C., and Grew, E.S. (1999) Crystal structure of boralsilite and its relation to a family of borosilicates, sillimanite and andalusite. *American Mineralogist*, 84, 1152–1161.
- Pieczka, A., Evans, R.J., Grew, E.S., Groat, L.A., Ma, C., and Rossman, G.R. (2013) The dumortierite supergroup. I. A new nomenclature for the dumortierite and hollite groups. *Mineralogical Magazine*, 77, 2825–2839.
- Pöter, B., Werdning, G., Schreyer, W., and Bernhardt, H.J. (1998) Synthesis and properties of the new borosilicate mineral boralsilite. *Berichte der Deutschen Mineralogischen Gesellschaft*, 1, 220.
- Schneider, H., Schreuer, J., and Hildmann, B. (2008) Structure and properties of mullite—A review. *Journal of the European Ceramic Society*, 28, 329–344.
- Sheldrick, G.M. (2008) A short history of *SHELX*. *Acta Crystallographica*, A64, 112–122.
- Wadoski, E.R., Grew, E.S., and Yates, M.G. (2011) Compositional evolution of tourmaline-supergroup minerals from granitic pegmatites in the Larsemann Hills, East Antarctica. *Canadian Mineralogist*, 49, 381–405.
- Werdning, G., and Schreyer, W. (1984) Alkali-free tourmaline in the system  $\text{MgO-Al}_2\text{O}_3\text{-B}_2\text{O}_3\text{-SiO}_2\text{-H}_2\text{O}$ . *Geochimica et Cosmochimica Acta*, 48, 1331–1344.
- (1990) Synthetic dumortierite: its *PTX*-dependent compositional variations in the system  $\text{Al}_2\text{O}_3\text{-B}_2\text{O}_3\text{-SiO}_2\text{-H}_2\text{O}$ . *Contributions to Mineralogy and Petrology*, 105, 11–24.
- (1992) Synthesis and stability of werdingite, a new phase in the system  $\text{MgO-Al}_2\text{O}_3\text{-B}_2\text{O}_3\text{-SiO}_2$  (MABS), and another new phase in the ABS-system. *European Journal of Mineralogy*, 4, 193–207.
- (1996) Experimental studies on borosilicates and selected borates. In E.S. Grew and L.M. Anovitz, Eds., *Boron: Mineralogy, Petrology, and Geochemistry*, 33, p. 117–163 (second printing 2002). Reviews in Mineralogy, Mineralogical Society of America, Chantilly, Virginia.
- Wodara, U., and Schreyer, W. (2001) X-site vacant Al-tourmaline: a new synthetic end-member. *European Journal of Mineralogy*, 13, 521–532.

MANUSCRIPT RECEIVED JANUARY 19, 2016

MANUSCRIPT ACCEPTED APRIL 21, 2016

MANUSCRIPT HANDLED BY G. DIEGO GATTA